

## SUPPLEMENTARY MATERIAL 1 - EXPANDED METHODS

### Palynology

Palynomorphs were recovered from samples using a modified standard palynological process in which carbonate and silicate minerals were removed with 10% hydrochloric acid followed by 48% hydrofluoric acid. Samples were then passed through a 100 $\mu$ m sieve and the fine fractions containing organic microfossils were concentrated by centrifuging in lithium heteropolytungstate (2.1g/ml). Samples for light microscopy were oxidized with weak Schulze solution and acetolysis. Palynological processing also included the addition of exotic *Lycopodium* tablets to permit the calculation of palynomorph concentration. All residues were mounted in glycerine jelly. Specimens were observed with a Nikon Eclipse 80i microscope and imaged with a DXMF 1200 camera through a Plan Apo objective using Differential Interference Contrast where appropriate. Extended Depth of Field micrographs were created using Photoshop. Following Traverse (2007), 200 palynomorphs per sample were identified and counted (note, in some instances multiple samples from the same quarry were combined to reach 200) except in two instances, where 100 palynomorphs per sample were identified and counted (Table S3). Dinoflagellates were also identified concurrently but counted separately to the count of 200 palynomorphs. All identifications were made through consultation of the original descriptions and images. All residues and slides are housed in the Department of Paleobiology, National Museum of Natural History, Smithsonian Institution (see Table S2 for detailed locality data).

### Carbon Isotope Value of Pollen ( $\delta^{13}\text{C}_{\text{pollen}}$ )

Pollen samples for isotopic analysis were initially treated with HCl and HF as above, but not oxidized. All processing was completed in double distilled water. Pollen grains were concentrated through sieving alone. A pollen-water slurry of each sample was placed on a microscope slide using a steel and glass syringe. Pollen grains of *Cupressacites hiatipites*

(Cupressaceae), *Caryapollenites veripites* (Juglandaceae) and *Arecipites tenuiexinuous* (Arecaceae) were then isolated from the slurry at 200X under light microscope using an Eppendorf Transferrman micromanipulator. Approximately 30-40 grains were rinsed in nano-pure water, placed in a 0.4 ul drop of nano-pure water, and the drop applied to a spooling-wire microcombustion (SWiM) device interfaced with a ThermoFinnigan Delta V+ isotope ratio mass spectrometer (ThermoFinnigan, Bremen, Germany) following methods described in Nelson (2012).

Sample isotopic data were normalized to Vienna Peedee Belemnite (VPDB) using  $\delta^{13}\text{C}$  measurements of aliquots containing 5 nmol C of dissolved in-house standards (leucine and sorbitol) that were previously calibrated to USGS40 and USGS41. Expected precision and accuracy of pollen  $\delta^{13}\text{C}$  data were determined by measuring  $\delta^{13}\text{C}$  values of the leucine and sorbitol standards across a size series containing varying amounts of carbon, including 5, 2.5, 1.25, 0.625, 0.3125, and 0.15625 nmol C (Table S7). Blanks (nano-pure water to which pollen grains were added and then removed) were analysed along with samples; in all cases the  $\text{CO}_2$  yields of pollen-containing samples were > 5x those of blanks.

#### **Organic Carbon Content and Carbon Isotope Value of TOC And N-alkanes ( $\delta^{13}\text{C}_{\text{TOC}}$ , $\delta^{13}\text{C}_{\text{alkane}}$ )**

A portion of each sediment sample was ground to a fine powder, acidified with 10% hydrochloric acid to remove carbonate, and soluble salts were removed by diluting with deionized water. Carbon isotope ratios and weight percent total organic carbon (TOC) were measured in duplicate using a Costech ECS 4010 combustion elemental analyser (EA) coupled to a Thermo Delta XP isotope ratio mass spectrometer (IRMS) (see Baczynski et al., 2013 for detailed methods).

Leaf waxes (*n*-alkanes) were extracted from separate hand samples taken at all sites that produced  $\delta^{13}\text{C}_{\text{pollen}}$ , and  $\delta^{13}\text{C}_{\text{alkane}}$  values were measured using a Trace 1310 gas

chromatograph coupled via a GC Isolink and ConFlo IV to a MAT 253 IRMS (Thermo Fisher Scientific) as described in Baczynski et al. (2018).

Carbon isotope values are reported in delta notation and normalized to VPDB using USGS 40, Urea #1 (Indiana University, Bloomington, IN, USA), and in-house standard Peru mud. Replicate measurements of standards indicate a measurement precision of  $\pm 0.16\text{‰}$  ( $n=81$ ;  $1\sigma$ ). The mean standard deviation on replicate sample analyses is  $0.2\text{‰}$  ( $n = 57$ ).

$\delta^{13}\text{C}_{\text{alkane}}$  values were normalized to the VPDB scale using Mix A ( $n\text{-C}_{16}$  to  $n\text{-C}_{30}$ ; Arndt Schimmelmann, Indiana University) and the Uncertainty Calculator (Polissar and D'Andrea, 2014). Standard errors of the mean range from  $0.1\text{‰}$  to  $0.2\text{‰}$  for individual samples.

### **Grain Size**

One-gram samples were treated with hot hydrogen peroxide to oxidize organic matter and treated with sodium metaphosphate to disaggregate them before particle size analysis (0.01-2000 microns) on the Malvern Mastersizer 3000 laser diffraction particle size analyzer was undertaken. All grain size analysis was completed at INSTAAR, University of Colorado Boulder by Wendy Roth.

### **Sample Ages**

Sample ages were calculated from stratigraphic elevation assuming uniform long-term sedimentation between the following calibration points: bases of Chron 25r (58.96 Ma), C25n (57.66), C24r (57.1), base of the CIE (55.93), end of body of CIE (55.832), end of rapid recovery of CIE (55.81), and top of Chron24r (53.899). Ages of calibration points are from Westerhold et al. (2018); stratigraphic elevations are from Clyde et al. (2007), Baczynski et al. (2013), Bowen et al. (2015), and van der Meulen et al. (2020).

## References

- Baczynski, A.A., McInerney, F.A., Wing, S.L., Kraus, M.J., Bloch, J.I., Boyer, D.M., Secord, R., Morse, P.E., and Fricke, H.C., 2013, Chemostratigraphic implications of spatial variation in the Paleocene-Eocene Thermal Maximum carbon isotope excursion, SE Bighorn Basin, Wyoming: *Geochemistry, Geophysics, Geosystems*, v. 14(10), p. 4133-4152, doi: [10.1002/ggge.20265](https://doi.org/10.1002/ggge.20265)
- Baczynski, A. A., Polissar, P. J., Juchelka, D., Schwieters, J., Hilkert, A., Summons, R. E., and Freeman, K. H., 2018, Picomolar-scale compound-specific isotope analyses: Rapid Communications in Mass Spectrometry, v. 32(9), p. 730-738, doi: [10.1002/rcm.8084](https://doi.org/10.1002/rcm.8084)
- Bowen, G.J., Maibauer, B.J., Kraus, M.J., Röhl, U., Westerhold, T., Steimke, A., Gingerich, P.D., Wing, S.L., and Clyde, W.C., 2015, Two massive, rapid releases of carbon during the onset of the Palaeocene–Eocene thermal maximum: *Nature Geoscience*, v. 8(1), p. 44-47, doi: [10.1038/ngeo2316](https://doi.org/10.1038/ngeo2316)
- Clyde, W.C., Hamzi, W., Finarelli, J.A., Wing, S.L., Schankler, D., and Chew, A., 2007, Basin-wide magnetostratigraphic framework for the Bighorn Basin, Wyoming: *Geological Society of America Bulletin*, v. 119(7-8), p. 848-859, doi: [10.1130/B26104.1](https://doi.org/10.1130/B26104.1)
- Nelson, D.M., 2012, Carbon isotopic composition of Ambrosia and Artemisia pollen: assessment of a C3-plant paleophysiological indicator: *New Phytologist*, v. 195(4), p. 787-793, doi: [10.1111/j.1469-8137.2012.04219](https://doi.org/10.1111/j.1469-8137.2012.04219)
- Polissar, P.J. and D'Andrea, W.J., 2014. Uncertainty in paleohydrologic reconstructions from molecular  $\delta D$  values. *Geochimica et Cosmochimica Acta*, v. 129, pp.146-156, doi: [10.1016/j.gca.2013.12.021](https://doi.org/10.1016/j.gca.2013.12.021)
- Traverse, A., 2007. *Paleopalynology*, v. 28. Springer Science & Business Media.
- van der Meulen, B., Gingerich, P. D., Lourens, L. J., Meijer, N., van Broekhuizen, S., van Ginneken, S., and Abels, H. A., 2020, Carbon isotope and mammal recovery from extreme greenhouse warming at the Paleocene–Eocene boundary in astronomically-calibrated fluvial strata, Bighorn Basin, Wyoming, USA: *Earth and Planetary Science Letters*, v. 534, p. 116044, doi: [10.1016/j.epsl.2019.116044](https://doi.org/10.1016/j.epsl.2019.116044)
- Westerhold, T., Röhl, U., Donner, B., and Zachos, J.C., 2018, Global extent of early Eocene hyperthermal events: A new Pacific benthic foraminiferal isotope record from Shatsky Rise (ODP Site 1209): *Paleoceanography and Paleoclimatology*, v. 33(6), p. 626-642, doi: [10.1029/2017PA003306](https://doi.org/10.1029/2017PA003306)

## SUPPLEMENTARY MATERIAL 2 - TAXONOMIC CONSIDERATIONS

It is possible that pollen morphotypes may represent two or more related biological species. In this study, grains of *Cupressacites hiatipites* Nichols 2010 may be derived from two ecologically similar 'taxodioid' conifers (family Cupressaceae), *Metasequoia occidentalis* and *Glyptostrobus europaeus*. Each is known from fossil shoots and cones at Paleocene and post-PETM Eocene sites (Wing and Currano, 2013). Grains of *Caryapollenites veripites* Nichols and Ott 1978 may or may not represent dispersed grains of more than one biological species. Four types of juglandaceous fruits have been recovered from the Paleocene sites we sampled for pollen: *Cruciptera*, *Polyptera*, *Cyclocarya*, and *Juglandicarya*. The first three

genera have pollen more like extant *Pterocarya*, but pollen of *Juglandicarya* is not known, so could be *Caryapollenites* (Manchester 1991; Manchester and Dilcher 1982; 1997). Only a single type of *Juglandicarya* fruit has been recovered from Bighorn Basin Paleocene-Eocene rocks (Wing and Currano, 2013). *Arecipites tenuiexinus* Leffingwell 1970 might have been produced by more than one species. The megafossil record of palms in the Paleocene-Eocene of the Bighorn Basin consists entirely of palm leaves (*Sabalites*) which have not been assigned to species.

## References

- Manchester, S.R. and Dilcher, D.L., 1982. Pterocaryoid fruits (Juglandaceae) in the Paleogene of North America and their evolutionary and biogeographic significance. *American Journal of Botany*, 69(2), p. 275-286, doi: [0.1002/j.1537-2197.1982.tb13258.x](https://doi.org/10.1002/j.1537-2197.1982.tb13258.x)
- Manchester, S.R. and Dilcher, D.L., 1997. Reproductive and vegetative morphology of Polyptera (Juglandaceae) from the Paleocene of Wyoming and Montana. *American Journal of Botany*, 84(5), p. 649-663, doi: [10.2307/2445902](https://doi.org/10.2307/2445902)
- Manchester, S.R., 1991. Cruciptera, a new juglandaceous winged fruit from the Eocene and Oligocene of western North America. *Systematic Botany*, p.715-725, doi: 10.2307/2418873
- Wing, S. L., and Currano, E. D., 2013, Plant response to a global greenhouse event 56 million years ago: *American Journal of Botany*, v. 100(7), p. 1234-1254, doi: [10.3732/ajb.1200554](https://doi.org/10.3732/ajb.1200554)

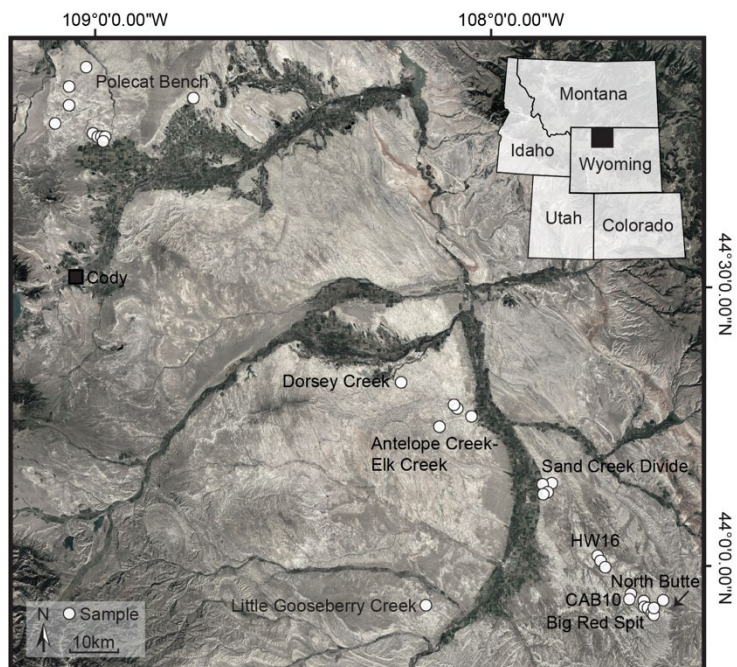


**Figure S1.** Map of the Bighorn Basin showing the location of samples (white circles) at which spore-pollen,  $\delta^{13}\text{C}_{\text{TOC}}$ , and  $\delta^{13}\text{C}_{\text{alkane}}$  values were measured. Locality names indicate detailed Paleocene-Eocene Thermal Maximum stratigraphic sections (Baczynski et al. 2016).

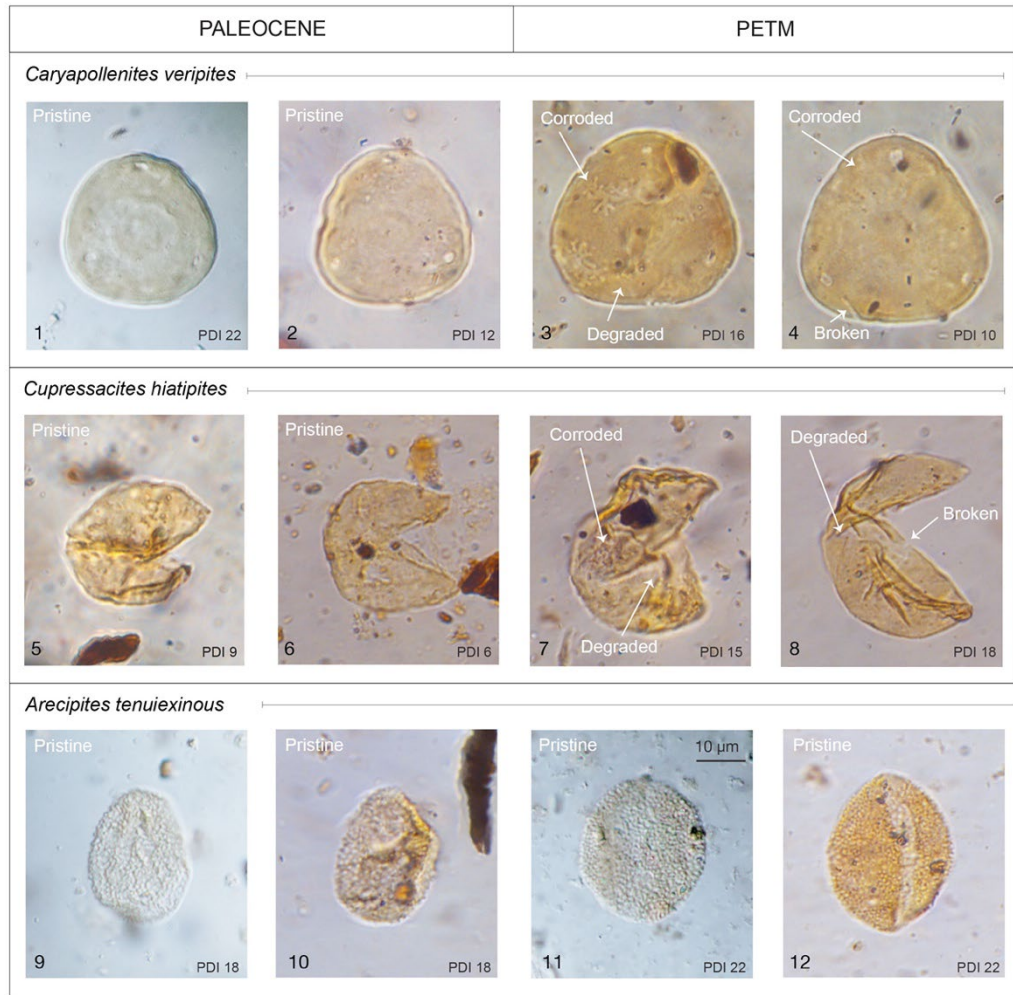


**Figure S2.** Variable preservation and Palynomorph Darkness Index (PDI) of pollen during the latest Paleocene and the body of the PETM/CIE. Thermal maturity of grains was assessed using the Palynomorph Darkness Index (PDI) of Goodhue and Clayton (2010). Grains with an etched or pitted exine are classified as corroded, those in which the sculptural and structural details of exine are difficult to resolve are classified as degraded, and those with a ruptured exine are classified as broken. Scale bar on all figures 10 µm. **1-2.** *Caryapollenites veripites*, SLW9417, Paleocene. **3-4.** *Caryapollenites veripites*, SLW0601, Eocene, body of CIE. **5-6.** *Cupressacites hiatipites*, SLW9901, Paleocene. **7-8.** *Cupressacites hiatipites*, PS1606, Eocene, body of CIE. **9-10.** *Arecipites tenuixinous*, SLW1612, Paleocene. **11-12.** *Arecipites tenuixinous*, PS0504, Eocene, body of CIE.

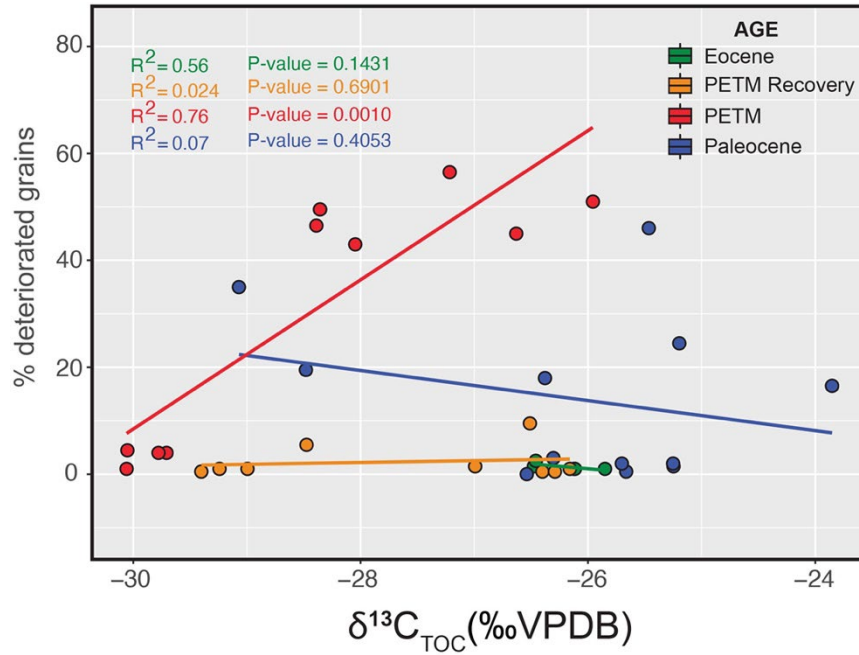


**Figure S3.** Relationship between  $\delta^{13}\text{C}_{\text{TOC}}$  values and the proportion of deteriorated pollen before, during, and after the PETM. The single anomalously high value of  $-19.9\text{‰}$  in the post-PETM early Eocene is not included in this analysis because it likely results from contamination by abundant carbonate shell fragments in the sample. Only during the body of the CIE is there a significant relationship between the percent of deteriorated grains in a sample and its  $\delta^{13}\text{C}_{\text{TOC}}$ . This is because organic matter from the Paleocene was 4-5‰ less negative than organic matter from the body of the CIE (Baczynski et al., 2013, 2018). Samples with a higher proportion of deteriorated (reworked) Paleocene or older pollen also have a higher proportion of Paleocene or older organic matter, and therefore a less negative isotopic composition than samples with organic matter fixed during the body of the CIE.